SCIENCE CHINA
Technological Sciences

• Article •

May 2014 Vol.57 No.5: 1030–1039
doi: 10.1007/s11431-014-5538-9

Equilibrium scour depth at offshore monopile foundation in combined waves and current

QI WenGang & GAO FuPing*

Key Laboratory for Mechanics in Fluid Solid Coupling Systems, Institute of Mechanics, Chinese Academy of Sciences, Beijing 100190, China

Received December 16, 2013; accepted March 22, 2014; published online April 17, 2014

Unlike the pier scour in bridge waterways, the local scour at offshore monopile foundations should take into account the effect of wave-current combination. Under the condition of wave-current coexistence, the water-soil interfacial scouring is usually coupled with the pore-pressure dynamics inside of the seabed. The aforementioned wave/current-pile-soil coupling process was physically modeled with a specially designed flow-structure-soil interaction flume. Experimental results indicate that superimposing a current onto the waves obviously changes the pore-pressure and the flow velocity at the bed around the pile. The concomitance of horseshoe vortex and local scour hole around a monopile proves that the horseshoe vortex is one of the main controlling mechanisms for scouring development under the combined waves and current. Based on similarity analyses, an average-velocity based Froude number (Fr_a) is proposed to correlate with the equilibrium scour depth (S/D) at offshore monopile foundation in the combined waves and current. An empirical expression for the correlation between S/D and Fr_a is given for predicting equilibrium scour depth, which may provide a guide for offshore engineering practice.

monopile, pore-pressure, scour depth, combined waves and current, Froude number

Citation: Qi W G, Gao F P. Equilibrium scour depth at offshore monopile foundation in combined waves and current. Sci China Tech Sci, 2014, 57: 1030–1039, doi: 10.1007/s11431-014-5538-9

1 Introduction

With the growing renewable energy needs around the world, offshore wind energy is fast becoming an attractive proposition in the last two decades for its rich resources, close proximity to electricity demand centers and little impact on local communities. China owns 200 GW wind energy capacity at the height of 50 m above the sea level in the inshore areas within the water depth of 5–25 m [1]. A target of 30 GW ambitious plans for large-scale offshore wind energy development has been proposed by 2020 in China, which makes the nation emerging as the second global hotspot after Europe for offshore wind development [2]. The dimensions of the offshore wind turbines are huge (as large as 90–150 m), posing significant challenge in the design and construction of the foundations and making the foundations account for approximately 20%–30% of total offshore wind farm project costs [3,4].

At present, monopile foundation is the most popular foundation type for offshore wind turbines in shallow to medium-deep waters. The diameter of the monopile can be up to approximately 4–7 m to bear the huge loads and bending moment in the offshore environments. The large diameter of the monopile mainly brings two effects. On one hand, the large diameter makes the corresponding KC number relatively small with a typical range of 0–10. The Keulegan-Carpenter number (KC) is defined as

$$KC=U_{wm}T/D, \quad (1)$$

where U_{wm} is the maximum velocity of the undisturbed wave-induced oscillatory flow at the sea bottom above the

*Corresponding author (email: fpgao@imech.ac.cn)

wave boundary layer; D is the pile diameter; T is the wave period. On the other hand, small slenderness ratio (i.e. the ratio of pile embedment length to its diameter is normally around 5) leads to that the maximum scour depth could be up to 25% of the pile embedment length [4]. As such, the bearing capacity of the large-diameter monopile is quite sensitive to the water-soil interfacial scouring development and the pore-pressure dynamics inside of the seabed.

Unlike the pier scour in bridge waterways, the local scour at offshore monopile foundations should take into account the effects of wave-current combination. In the offshore environments, waves generally coexist with current [5], propagating either along or against the current. This makes the soil response around the pile more complicated than that due to waves or current alone. From the viewpoint of engineering practice, it is vitally important to better understand the fluid-pile-soil coupling mechanism and acquire the knowledge of pore-pressure response around the pile. Meanwhile, the scour depth prediction at a monopile foundation is attracting more and more attention [6–11]. Nowadays different offshore standards [12] propose the use of the equation in ref. [13] (see eq. (2)) for scour depth prediction around offshore wind turbines under the combined waves and current. This equation originates from the database of scour around a pile under waves alone and can thus produce a great inaccuracy [14]. It is of great significance to accurately predict the equilibrium scour depth around a monopile in the combined waves and current for practical engineering.

Numerous scour equations around a pile in steady current have been developed since more than half a century ago. Most studies focus on the scour of noncohesive sediment, in spite of many studies on the erosion of cohesive sediment by flow [15]. Melville and Sutherland equation [16] and the Colorado State University (CSU) equation [17] are two of the most commonly used scour equations. They give somewhat conservative estimates of scour depth, the former perhaps more so than the latter [18]. Other well-known scour equations are presented in refs. [19–23]. The accuracy of the equations was evaluated and compared in refs. [18,24]. A comprehensive description of scour around pile in steady current can be found in refs. [25–27].

For scour depth around pile exposed to waves alone, the number of prediction equation is much small compared with that under steady current. Sumer et al. [13] conducted a large number of experiments and found the following expression for the equilibrium scour depth in the live-bed condition:

$$S/D \approx 1.3[1-\exp(-0.03(KC-6))], \quad \text{for } KC \geqslant 6, \tag{2}$$

where S is the equilibrium scour depth at the pile. Dey et al. [28] presented the results of equilibrium scour depths at circular piles in clay and sand-clay mixed beds under waves alone. The variation of equilibrium scour depth with KC for different soil conditions follows an exponential law, as was given by Sumer et al. [13], having different coefficients and exponents. Recently, Zanke et al. [29] proposed the following unifying equation for the prediction of equilibrium scour depth around a pile under the action of waves, tidal or steady currents:

$$S/D = 2.5(1-0.5\ U_{cr}/U)\ x_{rel}, \tag{3}$$

where $x_{rel}=x_{eff}/(1+x_{eff})$, $x_{eff} = 0.03(1-0.35U_{cr}/U)\ (KC-6)$, U is the mean velocity in case of steady currents, and U_{cr} is the critical velocity for initiation of sediment motion. Recent reviews of the subject were put forward in refs. [26,27].

The coexistence of waves and current is the most usual condition for shallow-water subsea locations. Nevertheless, the related research is relatively few. Sumer and Fredsøe [30] conducted a series of tests of irregular waves propagating either along or perpendicular to the current, indicating that the scour depth under the combined waves and current is influenced by the KC number and the ratio of velocities (U_{cw}, defined in eq. (8)). Sumer and Fredsøe [27] carried out reanalysis of scour data in ref. [30] and derived the following empirical expression for the scour depth under the combined waves and current:

$$S/D=S_c/D\{1-\exp[-A(KC-B)]\}, \ \text{for} \ KC \geqslant B, \tag{4}$$

in which S_c is the scour depth for the current-only case, and the parameters A and B are given as $A=0.03+0.75U_{cw}^{2.6}$ and $B=6\exp(-4.7U_{cw})$. The range of validity of eq. (4) is limited to $4<KC<25$. Eq. (4) is the only prediction equation for the condition of the combined waves and current. Yet the variation range of S_c/D is very large, producing a great arbitrariness and uncertainty in the practical engineering application; and the accuracy of eq. (4) is not very much optimistic [31]. Recently, Sumer et al. [32] presented some new experimental scour data under the combined waves and current. Qi and Gao [33] conducted an experimental investigation of the local scour development under the combined waves and current at a monopile. The influence of the wave propagating direction relative to current is obvious. The interaction between scour development and pore-pressure response around the pile was discussed.

The aforementioned studies on the scour prediction around a pile under the combined waves and current mainly focused on the cases with relatively large KC numbers ($KC>4$), while the typical value of the KC number for monopiles in practical offshore situations is relatively small. No accurate prediction model for equilibrium scour depth around a pile under the combined waves and current has been established.

In this study, the wave/current-pile-soil coupling process of local scour around monopole foundation was physically modeled with a specially designed water flume. Based on similarity analysis, a series of flume tests were conducted to investigate the pore-pressure response and the scouring development around the test pile in the combined waves and current.

2 Similarity analyses and physical modeling

2.1 Similarity analyses

The local scour around a pile under the combined waves and current involves a complex interaction between wave/current, pile and its neighboring soil. It is of significant importance to identify the non-dimensional variables that play the most relevant role on the scour around a pile under the combined waves and current.

For the local scour around a pile in the combined waves and current, there exist many pertinent parameters characterizing the pile, sand-bed, fluid properties and hydrodynamic loads. The pile properties can be characterized by its diameter (D). The sand-bed properties can be summarized by median diameters of soil (d_{50}), geometric standard deviation of grain size distribution (σ_g), sediment grain density (ρ_s), coefficient of permeability (k_s), shear modulus of soil skeleton (G), and degree of saturation (S_r). The fluid physical properties can be characterized by water density (ρ_w) and kinematic viscosity of water (ν). The wave-current combined oscillatory flow can be characterized by water depth (h), wave period (T), maximum velocity of the undisturbed wave-induced oscillatory flow at the sea bottom above the wave boundary layer (U_{wm}), and representative near-bed velocity of the current component of the undisturbed combined flow (U_c). The gravitational acceleration (g) is included among the variables due to the presence of a free surface and the different density between the sediment and water. Based on the aforementioned analysis, the equilibrium scour depth (S) can be described by the following functional relationship:

$$S = f(D, d_{50}, \sigma_g, \rho_s, k_s, G, S_r, \rho_w, \nu, h, T, U_{wm}, U_c, g, \cdots). \quad (5)$$

There is no general agreement on what specific set of dimensionless parameters should be utilized. It can be argued that a typical set of dimensionless parameters should include subsets to represent the interactions between fluid-flow and pile, between fluid-flow and sediment, and the relative size of the representative current velocity to representative wave velocity [34]. Therefore, based on the Buckingham Pi-Theorem in the dimensional analysis, choosing D, g and G as the repeating variables, the equilibrium scour depth normalized with pile diameter can be expressed in the following non-dimensional forms:

$$\frac{S}{D} = f\left(Fr_a, KC, U_{cw}, Re, \theta, \frac{k_s G}{\rho_w g^2 T h}, S_r, \frac{D}{d_{50}}, \frac{h}{D}, \frac{\rho_s}{\rho_w}, \sigma_g \cdots\right), \quad (6)$$

in which the average-velocity based Froude number (Fr_a), the ratio of velocities (U_{cw}), the pile Reynolds number (Re) and the Shields parameter (θ) are defined as follows, respectively:

$$Fr_a = U_a / \sqrt{gD}, \quad (7)$$

$$U_{cw} = U_c / (U_c + U_{wm}), \quad (8)$$

$$Re = U_m D / \nu, \quad (9)$$

$$\theta = \frac{U_f^2}{g(\rho_s / \rho_w - 1) d_{50}}, \quad (10)$$

in which

$$U_a = \left(\frac{1}{T/4} \int_0^{T/4} \left(U_c + U_{wm} \sin(2\pi t / T)\right) \mathrm{d}t = U_c + \frac{2}{\pi} U_{wm} \right)$$

is the average water particle velocity during one-quarter cycle of oscillation under the combined waves and current when the oscillatory motion and the current are in the same direction; U_m ($=U_c+U_{wm}$) is the maximum value of the combined waves and current velocity at the level of $1.0D$ above the sand-bed; and U_f is the maximum value of the undisturbed friction velocity, which can be calculated from the variables in eq. (5) characterizing the sand-bed properties, fluid physical properties and wave-current combined oscillatory flow [35].

The parameter Fr_a in eq. (7) is a newly proposed pile Froude number definition under the combined waves and current, based on the average water particle velocity (U_a). The dependence of S/D on Fr_a will be detailed in Section 3.2.

The ratio of velocities (U_{cw}) has been proved to be an important dimensionless parameter [30]. The Keulegan-Carpenter number (KC) is the controlling parameter for vortex generation and development around a cylindrical structure in waves, which was used for correlation with the scour depth around a pile under the action of waves alone and waves plus current [13,30].

In the present tests, the pile Reynolds number is approximately $O(10^4)$, so the flow around the test pile is turbulent. The effect of pile Reynolds number is usually negligible for turbulent flow [36].

The Shields parameter (θ) is a non-dimensional shear stress at the surface of sediments in a flow, whose physical meaning is the ratio of fluid force on the particle to the weight of the particle. The detailed calculation procedure of θ under the combined waves and current was given by Soulsby [35]. The variation of the scour depth with θ at the bridge pier in a steady flow was given by Melville and Coleman [37]. Under the combined waves and current, the wave-induced upward seepage force makes the sand grains easier to be lifted, the bed more vulnerable to motion, i.e. decreasing the critical Shields parameter (θ_{cr}) and making the bed surface more susceptible to the scour [38].

The dimensionless parameters $\frac{k_s G}{\rho g^2 T h}$ and S_r have decisive influence on the wave-induced pore-pressure development in the soil [30]. The possibility of soil liquefying becomes greater as $\frac{k_s G}{\rho g^2 T h}$ and S_r get smaller [33].

According to Melville and Chiew [39], D/d_{50} barely has effect on the scour development for $D/d_{50}>50$. However, some more recent research indicates a decrease in S/D at very large values of D/d_{50} [40,41]. Consequently, a prototype scour depth predicted based on the flume scour data is greater than that in practice, i.e. a relatively conservative or safe prediction value of scour depth should be expected. A reduction of the scour depth prediction should be fulfilled according to the dependence of scour depth on D/d_{50}.

h/D is the relative proportion of flow depth and pile diameter, which is useful for describing the interaction of the downflow into the scour hole and the horseshoe vortex around the pile [36,37]. ρ_s/ρ_w is the specific density of the sand and ρ_s/ρ_w=2.65 for the quartz sand. σ_g characterizes the gradation of the sediment.

2.2 Experimental set-up and procedure

The experiments were conducted in a flow-structure-soil interaction flume (52 m long, 1 m wide and 1.5 m high) at the Institute of Mechanics, Chinese Academy of Sciences. The water depth (h) was kept constant at 0.5 m, as illustrated in Figure 1. A saturated sand-bed was adopted to simulate a sandy seabed, whose main physical properties are listed in Table 1. The detailed information of the flume and sand-bed can be found in ref. [33].

Far-field wave height was measured with a wave height gauge along the central line at the distance 15 m apart from the pile. An Acoustic Doppler Velocimetry (ADV) was mounted to measure the undisturbed flow velocity at the level of 1.0D above the sand-bed at the distance 20 m apart from the pile centre. Four GE Druck miniature pore-pressure sensors were utilized to measure the pore-pressure at upstream and downstream pile edges. The scour depth evolution at upstream and downstream pile edges was monitored with two ultrasonic distance sensors.

Test conditions and scour measurements are summarized in Table 2 for current alone and current with following waves, and Table 3 for current with opposing waves. The scour depth, pore-pressure response around the pile, wave height and flow velocity were measured simultaneously. Low KC number conditions are more common in the practice and related study for waves-current combined condition is scarce. Thus the KC number in the present experiments lies in the range 0 to 4.

The variable quantities U_c and U_{wm} in Tables 2 and 3 are individually the velocity of the current component and orbital component of the undisturbed combined flow, measured at the level of 1.0D above the sand-bed, representing the characteristic flow velocity at the boundary layer.

The critical Shields parameter for the sediment initiation on the bed can be calculated by [35]

$$\theta_{cr}=\frac{0.3}{1+1.2D_*}+0.055\left[1-\exp\left(-0.02D_*\right)\right], \tag{11}$$

in which $D_*=d_{50}\left[\left(s-1\right)g/\nu^2\right]^{1/3}$ is known as the dimensionless grain size. For the present examined medium sand-bed, the value of θ_{cr} is 0.036. As shown in Tables 2 and 3, the live-bed scour regime prevailed in the present experiments except runs 1, 5 and 9.

3 Results and discussions

3.1 Pore-pressure response around the pile

Wave-induced pore-pressure could exert upward seepage force onto the particles at the wave troughs and even liquefy the soil around the pile [42]. Pore-pressure response around the pile under the action of waves is complicated for the interaction between the soil, impervious pile boundary, and vortices induced by pile blockage. Superimposing a current would further increase the complexity of this issue.

There usually exist two mechanisms for wave-induced pore-pressure response, including oscillatory pore-pressure and residual pore-pressure [43]. The build-up of pore-pressure (residual pore-pressure) has not been observed for the examined hydrodynamic loads and the medium sand, which might be due to high permeability of the test sands (see Table 1) [33].

The amplitudes of the pore-pressure at both the upstream pile edge and downstream pile edge under waves alone, waves with a following current, and waves with an opposing current, are shown in Table 4. The waves adopted in

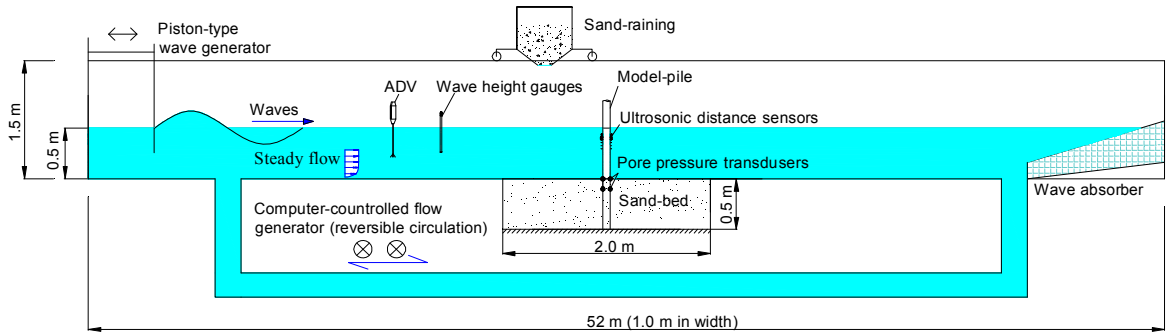

Figure 1 (Color online) Schematic diagram of the experimental system (not in scale).

Table 1 Index properties of test sands

Mean size of sand grains d_{50} (mm)	Geometric standard deviation σ_g	Coefficient of permeability k_s (m/s)	Void ratio e	Relative density D_r	Buoyant unit weight of soil γ' (kN/m^3)
0.38	1.28	1.88×10^{-4}	0.771	0.352	9.03

Table 2 Test results for local scour around a pile: Current alone and current with following waves

Run number	D (m)	H (m)	T (s)	U_c (m/s)	U_{wm} (m/s)	U_m (m/s)	U_{cw}	θ	KC	Re	Fr_a	S/D
1	0.20	0	1.40	0.15	0	0.15	1.00	0.008	–	2.21×10^4	0.107	0
2	0.20	0.043	1.40	0.15	0.068	0.218	0.69	0.036	0.48	3.21×10^4	0.138	0.025
3	0.20	0.097	1.40	0.15	0.137	0.287	0.52	0.075	0.96	4.22×10^4	0.169	0.075
4	0.20	0.145	1.40	0.15	0.201	0.351	0.43	0.125	1.41	5.16×10^4	0.199	0.11
5	0.20	0	1.40	0.23	0	0.23	1.00	0.02	–	3.38×10^4	0.164	0.20
6	0.20	0.026	1.40	0.23	0.063	0.293	0.78	0.036	0.44	4.31×10^4	0.193	0.27
7	0.20	0.052	1.40	0.23	0.107	0.337	0.68	0.054	0.75	4.96×10^4	0.213	0.34
8	0.20	0.085	1.40	0.23	0.156	0.386	0.6	0.078	1.09	5.68×10^4	0.235	0.44
9	0.08	0	1.40	0.23	0	0.23	1.00	0.021	–	1.35×10^4	0.26	0.39
10	0.08	0.033	1.40	0.23	0.073	0.303	0.76	0.045	1.28	1.78×10^4	0.312	0.65
11	0.08	0.068	1.40	0.23	0.126	0.356	0.65	0.07	2.21	2.09×10^4	0.35	0.84
12	0.08	0.103	1.40	0.23	0.173	0.403	0.57	0.104	3.03	2.37×10^4	0.384	1.00
13	0.08	0	1.40	0.34	0	0.34	1.00	0.049	–	2.00×10^4	0.384	1.15
14	0.08	0.098	1.40	0.34	0.157	0.497	0.68	0.124	2.75	2.92×10^4	0.497	1.26
15	0.20	0	1.40	0.34	0	0.34	1.00	0.049	–	5.00×10^4	0.243	0.62
16	0.20	0.057	1.40	0.34	0.104	0.444	0.77	0.075	0.73	6.53×10^4	0.29	0.67
17	0.20	0.092	1.40	0.34	0.14	0.48	0.71	0.104	0.98	7.06×10^4	0.307	0.65
18	0.08	0.108	1.80	0.20	0.117	0.317	0.63	0.066	2.63	1.86×10^4	0.310	0.73
19	0.08	0.112	1.80	0.22	0.129	0.349	0.63	0.077	2.90	2.05×10^4	0.341	0.70
20	0.08	0.056	1.80	0.26	0.087	0.347	0.75	0.065	1.96	2.04×10^4	0.356	1
21	0.08	0.084	2.00	0.107	0.090	0.197	0.54	0.039	2.25	1.16×10^4	0.186	0.33

Table 3 Test results for local scour around a pile: Current with opposing waves

Run number	D (m)	H (m)	T (s)	U_c (m/s)	U_{wm} (m/s)	U_m (m/s)	U_{cw}	θ	KC	Re	Fr_a	S/D
22	0.08	0.152	1.4	0.20	0.136	0.336	0.6	0.086	2.38	1.98×10^4	0.324	0.76
23	0.08	0.140	1.4	0.23	0.141	0.371	0.62	0.08	2.47	2.12×10^4	0.361	0.78
24	0.08	0.138	1.8	0.18	0.162	0.342	0.53	0.091	3.65	2.01×10^4	0.320	0.73
25	0.08	0.082	1.8	0.27	0.122	0.396	0.69	0.084	2.75	2.33×10^4	0.397	1.03
26	0.08	0.102	2.0	0.11	0.144	0.253	0.43	0.063	3.6	1.49×10^4	0.227	0.25
27	0.08	0.086	2.0	0.21	0.111	0.321	0.65	0.063	2.78	1.89×10^4	0.317	0.75
28	0.20	0.129	1.4	0.22	0.140	0.360	0.61	0.057	0.98	1.91×10^4	0.221	0.29

these various tests have exactly the same wave height and wave period (H_0=9.2 cm, T=1.4 s).

It is seen that under the condition of waves alone, the amplitudes of pore-pressure at the upstream pile edge are greater than those at the downstream pile edge (①>② in Table 4). This is attributed to the influence of the large-scale wake vortices (see Figures 2(a) and (b)). Since the diffraction parameter D/L (L is the wave-length) is relatively small in these tests (D/L<0.08), it is reasonable to assume that the upstream and downstream pile edges are always either in the wave crest area or wave trough area at the same moment, as shown in Figure 2. The waves induce a local flow nearby the pile, whose travelling direction is following the wave propagating direction in the wave crest area and opposing the wave propagating direction in the wave trough area. In the wave crest area, wake vortices occur at the downstream pile edge and produce a region of low pressure nearby the vortices, which could make the exerted maximum wave pressure at the bed near downstream pile edge decrease. Likewise, in the wave trough area, the minimum pore-pressure at the bed near the upstream pile edge will also get smaller due to the wake vortices. The decreased

Table 4 Amplitudes of the wave-induced seabed response at upstream and downstream pile edges (T=1.4 s, H_0=9.2 cm; U_c=0.17 m/s for following-current case and U_c=0.19 m/s for opposing-current case)

Testing condition	Waves alone		Waves with a following current		Waves with an opposing current	
Location	Upstream	Downstream	Upstream	Downstream	Upstream	Downstream
Depth (cm) \ Number	①	②	③	④	⑤	⑥
0	207.4	199.3	222.3	197.4	213.3	178.7
10	188.7	174.1	190.8	182.2	179.7	158

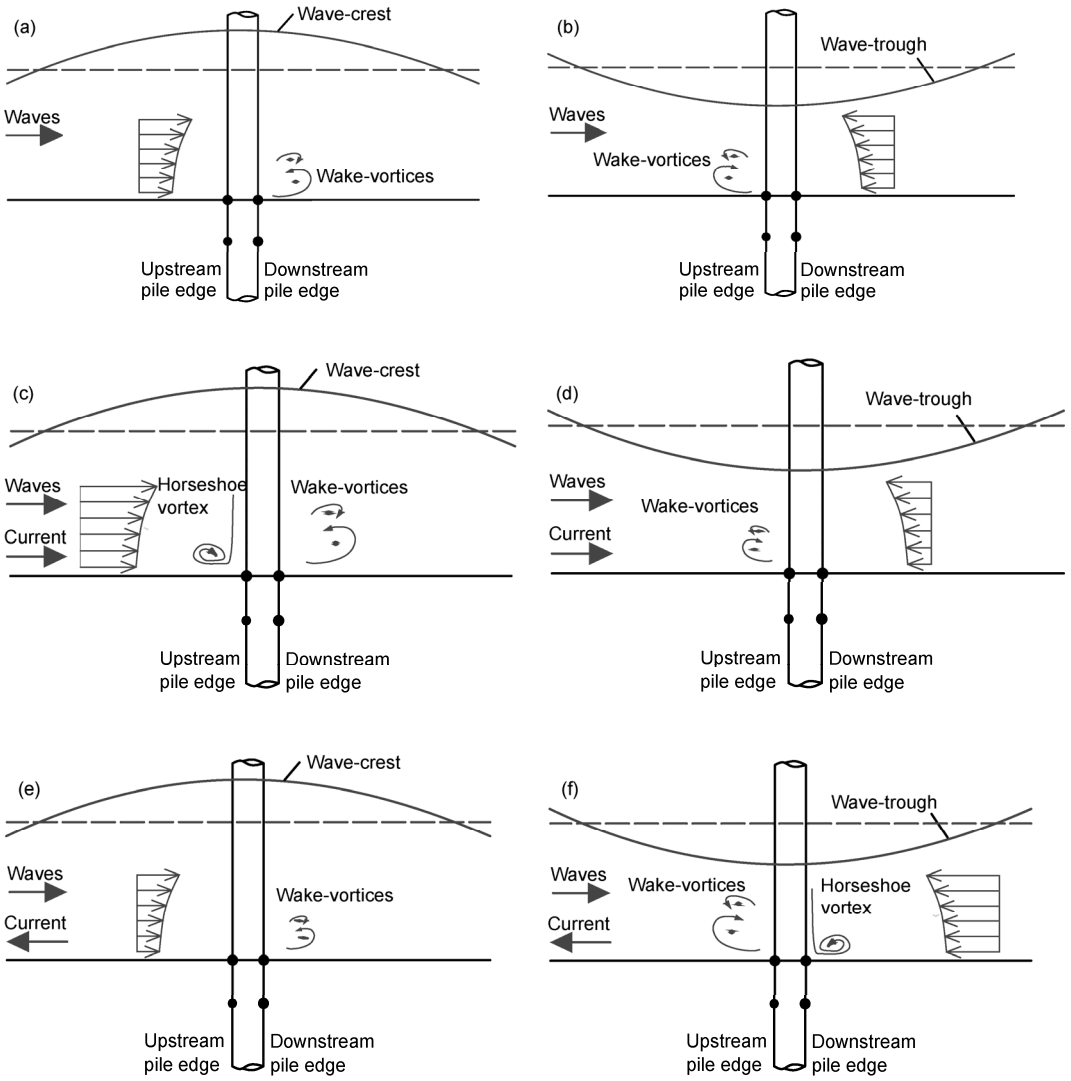

Figure 2 Illustration of coming flow and vortices around the pile. (a) Wave crest area under waves alone; (b) wave trough area under waves alone; (c) wave crest area under waves plus following current; (d) wave trough area under waves plus following current; (e) wave crest area under waves plus opposing current; (f) wave trough area under waves plus opposing current.

maximum wave pressure near the downstream pile edge and minimum wave pressure near the upstream pile edge altogether lead to larger pore-pressure amplitudes at the upstream pile edge.

The amplitude of far-field pore-pressure response increases after superimposing a following current and decreases after superimposing an opposing current [44]. The vortices structure nearby the pile under the combined waves and current would be different from those under waves alone. Under the action of waves and a following current, at the wave crest, the maximum value of the flow velocity increases (see Figure 2(c)). Thus the horseshoe vortex could emerge at the upstream pile side and wake vortices are intensified on the downstream pile side. The horseshoe vortex will exert an extra pressure load onto the bed [45,46] and increase the amplitude of the bed wave pressure, while the

intensified wave vortices will produce a region of low pressure and decrease the amplitude of the bed wave pressure. Considering the preceding effects of far-field pore-pressure response and vortices around the pile altogether, the pore-pressure amplitude at the bed increases at the upstream pile edge (③>① in Table 4) and decreases at the downstream pile edge (④<② in Table 4) after superimposing a following current onto the waves. Likewise, the pore-pressure amplitude at the bed also increases at the upstream pile edge (⑤>① in Table 4) and decreases at the downstream pile edge (⑥<② in Table 4) after superimposing an opposing current onto the waves (see Figures 2(e) and (f)).

The pore-pressure amplitudes at either upstream or downstream pile edge in 10 cm deep soil always obey the rule that a following current makes them increase and an opposing current makes them decrease. The variation of the pore-pressure amplitudes at pile edges due to superimposing a current is consistent with that at far-field soil. This is attributed to the fact that the soil response around the pile at a certain depth is a three-dimensional issue, and can be affected by not only the exerted bed pressure just above the soil, but also the response of the neighbouring soil.

3.2 Prediction of equilibrium scour depth based on Fr_a

According to similarity analysis, under the condition of the combined waves and current, the average-velocity based pile Froude number (Fr_a, see eq. (7)) could be a crucial dimensionless parameter to determine the equilibrium scour depth (see eq. (5)). In fact, for the case of current alone, the pile Froude number ($Fr = U_c/\sqrt{gD}$) has been proved to be a significant parameter controlling the scouring process around a pile [47]. Ettema et al. [36] concluded that *Fr* represented the flow gradients around the pile and was responsible for the formation of the horseshoe vortex, which was the main flow structure to initiate and maintain the scouring process. Ettema et al. [48] further revealed that *Fr* expressed the scale of wake vortices shed from a cylinder in a current, which was also a significantly important mechanism for scouring process. Moreover, several scour depth prediction models for piles under current were proposed as a function of *Fr* [49, 50], further confirming the crucial effect of *Fr* on the scour depth. It can be reasonably inferred that for the case of the combined waves and current, *Fr* may relate to the aforementioned flow structures such as horseshoe vortex and wake vortices, which are responsible for the scouring process. Dependence of *S*/*D* on *Fr* should be expected under the combined waves and current.

Umeda et al. [51] defined a dimensionless parameter A_0 to correlate with the scale of the horseshoe vortex around a cylindrical pile under the combined waves and current. The scale of the horseshoe vortex is characterized with the separation distance, x_s, associated with the formation of the horseshoe vortex at the phase when the oscillatory motion and the current are in the same direction. A_0 is calculated with

$$A_0 = \frac{U_a T/4}{D} = \frac{1}{D}\int_0^{T/4}\left(U_c + U_{wm}\sin(2\pi/T)\right)dt = KC\frac{2+\pi V_r}{4\pi}, \tag{12}$$

in which V_r ($=U_c/U_{wm}=U_{cw}/(1-U_{cw})$) is named current ratio. The physical meaning of A_0 is the ratio of the travel distance of water particle during one-quarter cycle of oscillation to the pile diameter. As indicated in Figure 3, A_0 correlates well with x_s (represented with hollow circle in Figure 3). The separation distance (x_s) is zero for A_0<0.5, which means that no horseshoe vortex exists for A_0 below 0.5.

The present scour depth data is also plotted as function of A_0 along with the scour data of Sumer and Fredsøe [30] and Sumer et al. [32]. It is indicated that the scour depth also tends to be nil for A_0 below 0.5. The critical value of A_0 for scour depth occurrence is consistent with that for horseshoe vortex occurrence. This coincidence proves that the horseshoe vortex plays a key role in governing the scour process under the combined waves and current.

As aforementioned, the horseshoe vortex around the pile could relate to *Fr*. Therefore, *S*/*D* should be closely dependent on *Fr* for the combined waves and current condition. The average water particle velocity during one-quarter cycle of oscillation (U_a) is adopted in the definition of *Fr* for the combined waves and current condition (see eq. (7)). This new definition of *Fr* is named the average-velocity based pile Froude number and symboled with Fr_a. By adopting U_a in the definition, Fr_a is correlated with A_0, which reflects the scale of the horseshoe vortex, and thus relates to the scour process.

The equilibrium scour depths (live-bed scour regime) under waves and current obtained from the present experiments are plotted as a function of Fr_a in Figure 4, along with those of Sumer and Fredsøe [30] and Sumer et al. [32]. The test conditions of the data set in Figure 4 are listed in

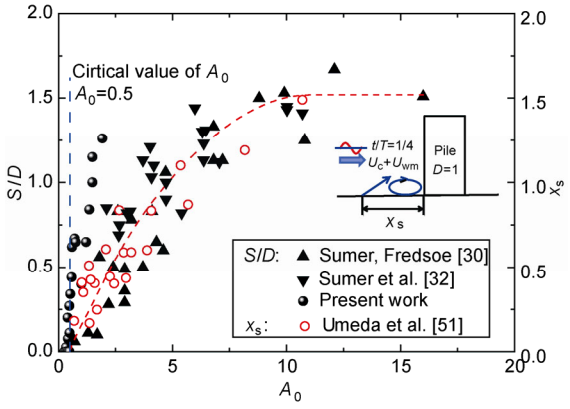

Figure 3 (Color online) Separation distance (x_s) and maximum scour depth in the equilibrium stage normalized with pile diameter (*S*/*D*) as function of A_0.

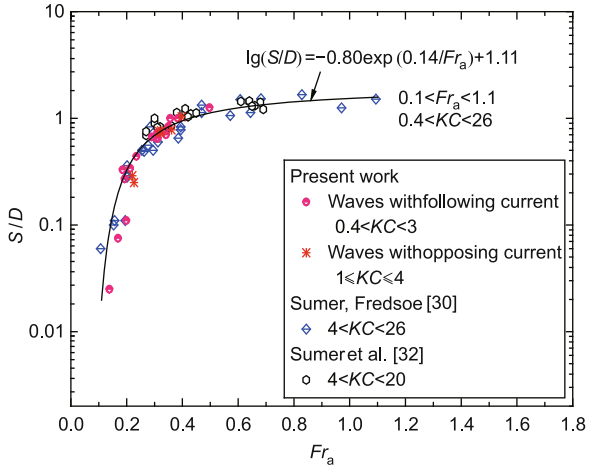

Figure 4 (Color online) Maximum equilibrium scour depth normalized with pile diameter (*S*/*D*) vs. the average-velocity based pile Froude number (Fr_a) for the combined waves and current.

Table 5 for Sumer and Fredsøe [30], and Table 6 for Sumer et al. [32], separately. No observable difference was detected between the following-current cases and opposing-current cases. There is a general and qualitative agreement between the present results and the results of the preceding studies, in spite of different ranges of *KC* values, water depth and sand grain size.

The scour depth data in Figure 4 can be formulated with the following empirical expression:

$$\lg(S/D) = -0.80\exp\left(0.14/Fr_a\right)+1.11,$$
$$\left(0.1 < Fr_a < 1.1,\ 0.4 < KC < 26\right). \quad (13)$$

Eq. (13) indicates that the scour depth approaches its mathematical asymptotic value ($S/D \approx 2.0$) as Fr_a increases (e.g., larger than 1.0). Note that this asymptotic value is in the range of a typical maximum scour depth prediction ($S/D \approx 1.7$ to 2.4) by previous local scour equations around a pile for current-alone conditions.

The accuracy of the data fitting with eq. (13) is evaluated by comparison with the present and the previous test results of scour depths. Figure 5 shows that approximately 85% of experimental data distribute in the range of 25% error lines. The present empirical prediction covers the examined *KC* range (0.4<*KC*<26) for the combined wave-current conditions.

Table 5 Existing test results and their test conditions of scour around a pile (reproduced from ref. [30])

Run number	D (m)	d_{50} (mm)	T (s)	U_{wm} (m/s)	U_c (m/s)	U_{cw}	KC	Fr_a	S/D
SF-1	0.090	0.16	2.50	0.157	0	0	4.36	0.106	0.06
SF-2	0.090	0.16	3.13	0.231	0	0	8.02	0.157	0.11
SF-3	0.030	0.16	3.23	0.242	0	0	26.02	0.284	0.83
SF-4	0.055	0.20	3.33	0.177	0	0	10.73	0.154	0.10
SF-5	0.032	0.20	3.33	0.177	0	0	18.44	0.201	0.36
SF-6	0.032	0.20	3.33	0.177	0	0	18.44	0.201	0.29
SF-7	0.032	0.20	3.33	0.177	0.03	0.14	18.44	0.255	0.50
SF-8	0.055	0.20	3.33	0.177	0.04	0.17	10.73	0.201	0.28
SF-9	0.032	0.20	3.33	0.177	0.06	0.26	18.44	0.312	0.60
SF-10	0.055	0.20	3.33	0.177	0.08	0.31	10.73	0.263	0.49
SF-11	0.090	0.16	2.50	0.157	0.08	0.35	4.36	0.195	0.11
SF-12	0.030	0.16	3.23	0.242	0.10	0.29	26.02	0.469	1.33
SF-13	0.090	0.16	3.13	0.231	0.13	0.36	8.02	0.295	0.50
SF-14	0.032	0.20	3.33	0.177	0.15	0.46	18.44	0.469	1.13
SF-15	0.090	0.16	2.50	0.157	0.16	0.50	4.36	0.277	0.56
SF-16	0.055	0.20	3.33	0.177	0.17	0.49	10.73	0.385	0.65
SF-17	0.030	0.16	3.23	0.242	0.18	0.42	26.02	0.607	1.50
SF-18	0.090	0.16	3.13	0.231	0.22	0.49	8.02	0.394	0.78
SF-19	0.032	0.20	3.33	0.177	0.27	0.60	18.44	0.682	1.53
SF-20	0.090	0.16	2.50	0.157	0.27	0.63	4.36	0.394	0.83
SF-21	0.030	0.16	3.23	0.242	0.30	0.55	26.02	0.828	1.67
SF-22	0.030	0.16	–	0	0.30	1.00	–	0.544	2.00
SF-23	0.055	0.20	3.33	0.177	0.36	0.67	10.73	0.644	1.13
SF-24	0.090	0.16	3.13	0.231	0.39	0.63	8.02	0.572	1.06
SF-25	0.090	0.16	–	0	0.39	1.00	–	0.415	1.21
SF-26	0.032	0.20	3.33	0.177	0.50	0.74	18.44	1.094	1.51
SF-27	0.055	0.20	3.33	0.177	0.60	0.77	10.73	0.971	1.25

Table 6 Existing test results and their test conditions of scour around a pile (reproduced from ref. [32])

Run number	D (m)	d_{50} (mm)	T (s)	U_{wm} (m/s)	U_c (m/s)	U_{cw}	KC	Fr_a	S/D
S-1	0.04	0.17	2.5	0.124	0.090	0.42	7.75	0.27	0.69
S-2	0.04	0.17	4.0	0.155	0.302	0.66	15.50	0.64	1.43
S-3	0.04	0.17	4.0	0.155	0.156	0.50	15.50	0.41	1.13
S-4	0.04	0.17	4.0	0.155	0.090	0.37	15.50	0.30	0.90
S-5	0.04	0.17	1.5	0.202	0.302	0.60	7.54	0.69	1.21
S-6	0.04	0.17	4.0	0.198	0.302	0.60	19.80	0.68	1.41
S-7	0.04	0.17	4.0	0.155	0.302	0.66	15.50	0.64	1.45
S-8	0.04	0.17	2.5	0.175	0.302	0.63	10.94	0.66	1.31
S-9	0.04	0.17	2.5	0.127	0.302	0.70	7.94	0.61	1.44
S-10	0.04	0.17	2.5	0.175	0.156	0.47	10.94	0.43	1.10
S-11	0.04	0.17	4.0	0.198	0.156	0.44	19.80	0.45	1.12
S-12	0.04	0.17	4.0	0.155	0.156	0.50	15.50	0.41	1.23
S-13	0.04	0.17	2.5	0.127	0.156	0.55	7.94	0.38	1.13
S-14	0.04	0.17	4.0	0.198	0.090	0.31	19.80	0.35	0.82
S-15	0.04	0.17	4.0	0.155	0.090	0.37	15.50	0.30	1.00
S-16	0.04	0.17	2.5	0.175	0.090	0.34	10.94	0.32	0.83
S-17	0.04	0.17	2.5	0.127	0.090	0.41	7.94	0.27	0.75
S-18	0.04	0.17	1.5	0.105	0.159	0.60	3.92	0.36	0.85
S-19	0.04	0.17	2.5	0.160	0.159	0.50	10.0	0.42	1.03
S-20	0.04	0.17	2.5	0.160	0.090	0.36	10.0	0.31	0.82
S-21	0.04	0.17	2.5	0.160	0.302	0.65	10.0	0.65	1.30

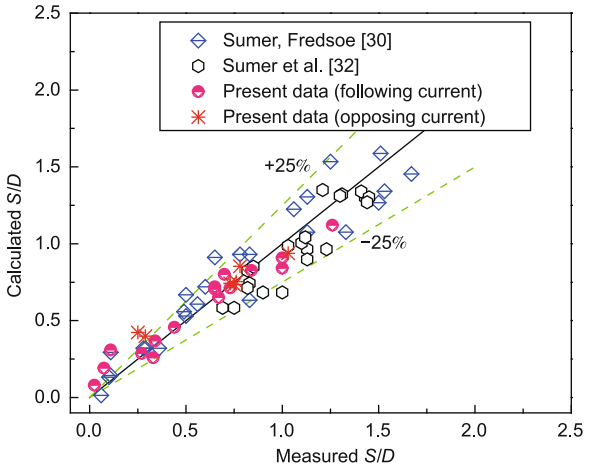

Figure 5 (Color online) Comparison of the measured and predicted scour depths. Live-bed scour regime ($\theta > \theta_{cr}$).

4 Conclusions

The local scour around a monopile foundation under the combined waves and current involves a complex interaction between wave/current, pile and its neighboring soil. Unlike the pier scour in bridge waterways, the local scour at offshore monopile foundations should take into account the effects of wave-current combination. Based on the similarity analysis, a series of large flume tests have been conducted to reveal the wave/current-pile-soil coupling physical mechanism and to predict the equilibrium scour depth at monopiles in the combined waves and current. The following conclusions are drawn.

1) Superimposing a current onto the waves obviously changes the pore-pressure and the flow velocity at the bed around the pile. The concomitance of horseshoe vortex and local scour hole around a pile proves that the horseshoe vortex is one of the controlling mechanisms for scouring development under the combined waves and current.

2) An empirical prediction model of equilibrium scour depth in the combined waves and current is established and matches well with the existing test data. This empirical model may provide a guide for offshore engineering practice.

3) The equilibrium scour depth (S/D) correlates well with the average-velocity based Froude number (Fr_a) for a wide range of KC number ($0.4<KC<26$). The equilibrium scour depth approaches an asymptotic value of $S/D \approx 2.0$ as Fr_a increases up to more than 1.0.

This work was supported by the National Natural Science Foundation of China (Grant Nos. 11232012, 10872198) and the National Basic Research Program of China ("973" Project) (Grant No. 2014CB046204).

1 Chen J J. Development of offshore wind power in China. Renew Sust Energ Rev, 2011, 15: 5013–5020
2 Hong L X, Möller B. Offshore wind energy potential in China: Under technical, spatial and economic constraints. Energy, 2011, 36: 4482–4491

3 Ernst & Young. Cost of and financial support for offshore wind. In: Ernst & Young Report for the Department of Energy and Climate Change, DECC, London, 2009
4 LeBlanc C. Design of offshore wind turbine support structures. Dissertation of Doctoral Degree. Denmark: TU of Denmark, 2004
5 Sørensen S P H, Ibsen L B, Frigaard P. Experimental evaluation of backfill in scour holes around offshore monopoles. In: Frontiers in Offshore Geotechnics II. Gourvenec S, White D, eds. London: Taylor & Francis Group, 2011. 617–622
6 Zhou Y R, Chen G P. Experimental study on local scour around a large circular cylinder under irregular waves. China Ocean Eng, 2004, 18: 245–256
7 Høgedal M, Hald T. Scour assessment and design for scour for monopile foundations for offshore wind turbines. In: Procedings of Copenhagen Offshore Wind, Copenhagen, 2005
8 Harris J, Whitehouse R J S, Benson T. The time evolution of scour around offshore structures. ICE–Maritime Eng, 2010, 163: 3–17
9 Whitehouse R J S, Harris J M, Sutherland J, et al. The nature of scour development and scour protection at offshore windfarm foundations. Mar Pollut Bull, 2011, 62: 73–88
10 Matutano C, Negro V, López–Gutiérrez J S, et al. Scour prediction and scour protections in offshore wind farms. Renew Energ, 2013, 57: 358–365
11 Chen L, Lam W H. Methods for predicting seabed scour around marine current turbine. Renew Sust Energ Rev, 2014, 29: 683–692
12 Det N V. DNV offshore standard DNV–OS–J101, design of offshore wind turbine. Technical Standard, 2013. 134–135
13 Sumer B M, Fredsøe J, Christiansen N. Scour around a vertical pile in waves. J Waterw Port C, 1992, 118: 15–31
14 Negro V, López–Gutiérrez J S, Esteban M D, et al. Uncertainties in the design of support structures and foundations for offshore wind turbines. Renew Energ, 2014, 63: 125–132
15 Zhu Y H, Lu J Y, Liao H Z, et al. Research on cohesive sediment erosion by flow: An overview. Sci China Ser E: Tech Sci, 2008, 51: 2001–2012
16 Melville B W, Sutherland A J. Design method for local scour at bridge piers. J Hydraul Eng, 1988, 114: 1210–1226
17 Richardson E V, Davis S R. Evaluating Scour at Bridges, Hydraulic Engineering Circular No. 18: US Fed Hwy Admin. US Dept Transp, FHWA–NHI–01–001, 2001
18 Johnson P A. Comparison of pier–scour equations using field data. J Hydraul Eng, 1995, 121: 626–629
19 Breusers H N C, Nicollet G, Shen H W. Local scour around cylindrical piers. J Hydraul Res, 1977, 15: 211–252
20 Froehlich D C. Analysis of onsite measurements of scour at piers. American Society of Civil Engineers National Conf on Hydraul Eng, Colorado Springs, CO, USA, 1988. 534–539
21 Kothyari U C, Garde R J, Ranga Raju K G. Temporal variation of scour around circular bridge piers. J Hydraul Eng, 1992, 118: 1091–1106
22 Melville B W. Pier and abutment scour: integrated approach. J Hydraul Eng, 1997, 123: 125–136
23 Sheppard D M, Odeh M, Glasser T. Large scale clear–water local pier scour experiments. J Hydraul Eng, 2004, 130: 957–963
24 Gaudio R, Grimaldi C, Tafarojnoruz A, et al. Comparison of formulae for the prediction of scour depth at piers. Proc 1st IAHR European Division Congress. Edinburgh, UK: Heriot-Watt University, 2010
25 Hoffmans G J C M, Verheij H J. Scour Manual. Rotterdam: A.A. Balkema, 1997
26 Whitehouse R. Scour at Marine Structures: A Manual for Practical Applications. London: Thomas Telford, 1998
27 Sumer B M, Fredsøe J. The Mechanics of Scour in the Marine Environment. Singapore: World Scientific, 2002
28 Dey S, Helkjær A, Mutlu Sumer B, et al. Scour at vertical piles in sand–clay mixtures under waves. J Waterw Port C, 2011, 137: 324–331
29 Zanke U C E, Hsu T W, Roland A, et al. Equilibrium scour depths around piles in noncohesive sediments under currents and waves. Coast Eng, 2011, 58, 986–991
30 Sumer B M, Fredsøe J. Scour around pile in combined waves and current. J Hydraul Eng, 2001, 127: 403–411
31 Rudolph D, Bos K J, Luijendijk A P, et al. Scour around offshore structures–analysis of field measurements. Proc 2nd International Conf on Scour and Erosion, Singapore, 2004. 14–17
32 Sumer B M, Petersen T U, Locatelli L, et al. Backfilling of a scour hole around a pile in waves and current. J Waterw Port C, 2013, 139: 9–23
33 Qi W G, Gao F P. Physical modeling of local scour development around a large-diameter monopile in combined waves and current. Coast Eng, 2014, 83: 72–81.
34 Cataño–Lopera Y A, Landry B J, García M H. Scour and burial mechanics of conical frustums on a sandy bed under combined flow conditions. Ocean Eng, 2011, 38: 1256–1268
35 Soulsby R. Dynamics of Marine Sands. London: Thomas Telford, 1997
36 Ettema R, Melville B W, Barkdoll B. Scale effect in pier–scour experiments. J Hydraul Eng, 1998, 124: 639–642
37 Melville B W, Coleman S E. Bridge Scour. Colorado: Water Resources Publications, 2000
38 Cheng N S, Chiew Y M. Incipient sediment motion with upward seepage. J Hydraul Res, 1999, 37: 665–681
39 Melville B W, Chiew Y M. Time scale for local scour at bridge piers. J Hydraul Eng, 1999, 125: 59–65
40 Sheppard D M, Odeh M, Glasser T. Large scale clear–water local pier scour experiments. J Hydraul Eng, 2004, 130: 957–963
41 Lee S, Sturm T. Effect of sediment size scaling on physical modeling of bridge pier scour. J Hydraul Eng, 2009, 135: 793–802
42 Li X J, Gao F P, Yang B, et al. Wave-induced pore-pressure responses and soil liquefaction around pile foundation. Int J Offshore Polar, 2011, 21: 233–239
43 Jeng D S, Seymour B, Gao F P, et al. Ocean waves propagating over a porous seabed: Residual and oscillatory mechanisms. Sci China Ser E: Tech Sci, 2007, 50: 81–89
44 Qi W G, Gao F P. Responses of sandy seabed under combined waves and current: Turbulent boundary layer and pore–water pressure. Proc of 8th International Conf on Physical Modelling in Geotechnic, Perth, Australia, 2014
45 Baker C J. The laminar horseshoe vortex. J Fluid Mech, 1979, 95: 347–367
46 Baker C J. The turbulent horseshoe vortex. J Wind Eng Ind Aerod, 1980, 6: 9–23
47 Shen H W, Schneider V R, Karaki S. Local scour around bridge piers. J Hydraul Div, 1969, 95: 1919–1940
48 Ettema R, Kirkil G, Muste M. Similitude of large–scale turbulence in experiments on local scour at cylinders. J Hydraul Eng, 2006, 132: 33–40
49 Olsen N R B, Kjellesvig H M. Three–dimensional numerical flow modelling for estimation of maximum local scour. J Hydraul Res, 1998, 36: 579–590
50 Debnath K, Chaudhuri S. Laboratory experiments on local scour around cylinder for clay and clay–sand mixed beds. Eng Geol, 2010, 111: 51–61
51 Umeda S, Yuhi M, Ishida H. Numerical study of three–dimensional flow fields around the base of a vertical cylinder in oscillatory plus mean flow. In: Proceedings of Coastal Structures 2003, Reston, 2003. 751–761